Positional stability of holographic optical traps

Arnau Farré,[1] Marjan Shayegan,[2] Carol López-Quesada,[1] Gerhard A. Blab,[3,4] Mario Montes-Usategui,[1] Nancy R. Forde,[3] Estela Martín-Badosa[1,*]

[1]*Optical Trapping Lab – Grup de Biofotònica, Departament de Física Aplicada i Òptica, Universitat de Barcelona, Martí i Franquès, 1 08028 Barcelona, Spain*

[2]*Department of Chemistry, Simon Fraser University, 8888 University Drive, Burnaby, British Columbia, V5A 1S6, Canada*

[3]*Department of Physics, Simon Fraser University, 8888 University Drive, Burnaby, British Columbia, V5A 1S6, Canada*

[4]*Current address: Molecular Biophysics, Universiteit Utrecht, Postbus 80000, 3508 TA Utrecht, The Netherlands*

**estela.martinb@ub.edu*

Abstract: The potential of digital holography for complex manipulation of micron-sized particles with optical tweezers has been clearly demonstrated. By contrast, its use in quantitative experiments has been rather limited, partly due to fluctuations introduced by the spatial light modulator (SLM) that displays the kinoforms. This is an important issue when high temporal or spatial stability is a concern. We have investigated the performance of both an analog-addressed and a digitally-addressed SLM, measuring the phase fluctuations of the modulated beam and evaluating the resulting positional stability of a holographic trap. We show that, despite imparting a more unstable modulation to the wavefront, our digitally-addressed SLM generates optical traps in the sample plane stable enough for most applications. We further show that traps produced by the analog-addressed SLM exhibit a superior pointing stability, better than 1 nm, which is comparable to that of non-holographic tweezers. These results suggest a means to implement precision force measurement experiments with holographic optical tweezers (HOTs).

OCIS codes: (140.7010) Laser trapping; (170.4520) Optical confinement and manipulation; (230.6120) Spatial light modulators; (350.4855) Optical tweezers.

References and links

1. Y. Hayasaki, M. Itoh, T. Yatagai, and N. Nishida, "Nonmechanical optical manipulation of microparticle using spatial light modulator," Opt. Rev. **6**(1), 24–27 (1999).
2. D. G. Grier, "A revolution in optical manipulation," Nature **424**(6950), 810–816 (2003).
3. A. Jesacher, S. Fürhapter, S. Bernet, and M. Ritsch-Marte, "Size selective trapping with optical "cogwheel" tweezers," Opt. Express **12**(17), 4129–4135 (2004).
4. T. Čižmár, M. Mazilu, and K. Dholakia, "In situ wavefront correction and its application to micromanipulation," Nat. Photonics **4**(6), 388–394 (2010).
5. K. Dholakia and T. Cizmar, "Shaping the future of manipulation," Nat. Photonics **5**(6), 335–342 (2011).
6. E. R. Dufresne and D. G. Grier, "Optical tweezer array and optical substrates created with diffractive optics," Rev. Sci. Instrum. **69**(5), 1974–1977 (1998).
7. J. E. Curtis, B. A. Koss, and D. G. Grier, "Dynamic holographic optical tweezers," Opt. Commun. **207**(1-6), 169–175 (2002).
8. R. Di Leonardo, F. Ianni, and G. Ruocco, "Computer generation of optimal holograms for optical trap arrays," Opt. Express **15**(4), 1913–1922 (2007).
9. P. Yeh and C. Gu, *Optics of Liquid Crystal Displays* (John Wiley & Sons Inc., 2009).
10. M. Reicherter, T. Haist, E. U. Wagemann, and H. J. Tiziani, "Optical particle trapping with computer-generated holograms written on a liquid-crystal display," Opt. Lett. **24**(9), 608–610 (1999).
11. A. van der Horst and N. R. Forde, "Calibration of dynamic holographic optical tweezers for force measurements on biomaterials," Opt. Express **16**(25), 20987–21003 (2008).
12. A. van der Horst, B. P. B. Downing, and N. R. Forde, "Position and intensity modulations in holographic optical traps created by a liquid crystal spatial light modulator," in *Optical Trapping Applications*, Vol. 1 of 2009 OSA Technical Digest (CD) (Optical Society of America, 2009), paper OMB3.

#151453 - $15.00 USD Received 21 Jul 2011; revised 17 Sep 2011; accepted 17 Sep 2011; published 13 Oct 2011

13. C. O. Mejean, A. W. Schaefer, E. A. Millman, P. Forscher, and E. R. Dufresne, "Multiplexed force measurements on live cells with holographic optical tweezers," Opt. Express **17**(8), 6209–6217 (2009).
14. A. Farré, A. van der Horst, G. A. Blab, B. P. B. Downing, and N. R. Forde, "Stretching single DNA molecules to demonstrate high-force capabilities of holographic optical tweezers," J. Biophotonics **3**(4), 224–233 (2010).
15. L. T. McLane, K. M. Carroll, J. Scrimgeour, M. D. Bedoya, A. Kramer, and J. E. Curtis, "Force measurements with a translating holographic optical trap," Proc. SPIE **7762**, 77621J, 77621J-10 (2010).
16. J. R. Moffitt, Y. R. Chemla, S. B. Smith, and C. Bustamante, "Recent advances in optical tweezers," Annu. Rev. Biochem. **77**(1), 205–228 (2008).
17. S. Serati and J. Harriman, "Spatial light modulator considerations for beam control in optical manipulation applications," Proc. SPIE **6326**, 63262W, 63262W-11 (2006).
18. A. Hermerschmidt, S. Osten, S. Krüger, and T. Blümel, "Wave front generation using a phase-only modulating liquid-crystal-based micro-display with HDTV resolution," Proc. SPIE **6584**, 65840E, 65840E-10 (2007).
19. J. R. Moore, N. Collings, W. A. Crossland, A. B. Davey, M. Evans, A. M. Jeziorska, M. Komarcevic, R. J. Parker, T. D. Wilkinson, and H. Xu, "The silicon backplane design for an LCOS polarization-insensitive phase hologram SLM," IEEE Photon. Technol. Lett. **20**(1), 60–62 (2008).
20. A. Lizana, A. Márquez, L. Lobato, Y. Rodange, I. Moreno, C. Iemmi, and J. Campos, "The minimum Euclidean distance principle applied to improve the modulation diffraction efficiency in digitally controlled spatial light modulators," Opt. Express **18**(10), 10581–10593 (2010).
21. E. Eriksson, S. Keen, J. Leach, M. Goksör, and M. J. Padgett, "The effect of external forces on discrete motion within holographic optical tweezers," Opt. Express **15**(26), 18268–18274 (2007).
22. M. Persson, D. Engström, A. Frank, J. Backsten, J. Bengtsson, and M. Goksör, "Minimizing intensity fluctuations in dynamic holographic optical tweezers by restricted phase change," Opt. Express **18**(11), 11250–11263 (2010).
23. D. J. McKnight, "Continuous view of dc-balanced images on a ferroelectric liquid-crystal spatial light modulator," Opt. Lett. **19**(18), 1471–1473 (1994).
24. A. Farré, C. López-Quesada, J. Andilla, E. Martín-Badosa, and M. Montes-Usategui, "Holographic optical manipulation of motor-driven membranous structures in living NG-108 cells," Opt. Eng. **49**(8), 085801 (2010).
25. I. Moreno, A. Lizana, A. Márquez, C. Iemmi, E. Fernández, J. Campos, and M. J. Yzuel, "Time fluctuations of the phase modulation in a liquid crystal on silicon display: characterization and effects in diffractive optics," Opt. Express **16**(21), 16711–16722 (2008).
26. F. Li, N. Mukohzaka, N. Yoshida, Y. Igasaki, H. Toyoda, T. Inoue, Y. Kobayashi, and T. Hara, "Phase modulation characteristics analysis of optically-addressed parallel-aligned nematic liquid crystal phase-only spatial light modulator combined with a liquid crystal display," Opt. Rev. **5**(3), 174–178 (1998).
27. Hamamatsu Photonics K. K., LCOS-SLM X10468 series -LC driving system- 2010.
28. K. Berg-Sørensen, L. Oddershede, E.-L. Florin, and H. Flyvbjerg, "Unintended filtering in a typical photodiode detection system for optical tweezers," J. Appl. Phys. **93**(6), 3167–3176 (2003).
29. S. F. Tolić-Nørrelykke, E. Schäffer, J. Howard, F. S. Pavone, F. Jülicher, and H. Flyvbjerg, "Calibration of optical tweezers with positional detection in the back focal plane," Rev. Sci. Instrum. **77**(10), 103101 (2006).
30. A. van der Horst and N. R. Forde, "Power spectral analysis for optical trap stiffness calibration from high-speed camera position detection with limited bandwidth," Opt. Express **18**(8), 7670–7677 (2010).
31. E. A. Abbondanzieri, W. J. Greenleaf, J. W. Shaevitz, R. Landick, and S. M. Block, "Direct observation of base-pair stepping by RNA polymerase," Nature **438**(7067), 460–465 (2005).
32. L. Nugent-Glandorf and T. T. Perkins, "Measuring 0.1-nm motion in 1 ms in an optical microscope with differential back-focal-plane detection," Opt. Lett. **29**(22), 2611–2613 (2004).
33. Y. Deng, J. Bechhoefer, and N. R. Forde, "Brownian motion in a modulated optical trap," J. Opt. A, Pure Appl. Opt. **9**(8), S256–S263 (2007).
34. K. Berg-Sørensen and H. Flyvbjerg, "Power spectrum analysis for optical tweezers," Rev. Sci. Instrum. **75**(3), 594–612 (2004).

1. Introduction

Since proposed in the late 1990s [1], the capabilities of holographic technology to precisely modulate the light of an optical trap in real time have awoken the interest of the optical trapping community. Holographic optical tweezers (HOTs) provide a powerful means to dynamically generate exotic beam shapes or complex 3D patterns of light foci for a wide variety of manipulation experiments [2–5].

The use of diffractive elements to split a laser beam into arrays of traps was first implemented by Dufresne and Grier [6]. A desired pattern of traps was obtained by placing a fixed, computer-generated hologram at a conjugate plane of the objective's entrance pupil. An improvement of this basic idea quickly followed with the introduction of a spatial light modulator (SLM) into the beam path. A phase kinoform on the liquid crystal (LC) display could be updated at video rate, which translated into real-time control of several traps

#151453 - $15.00 USD Received 21 Jul 2011; revised 17 Sep 2011; accepted 17 Sep 2011; published 13 Oct 2011

independently [7]. Different strategies to compute these kinoforms at high rates have been reported and a wide choice of algorithms that optimize several performance metrics is currently available [5,8].

Parallel nematic liquid crystal SLMs provide a simple way to modulate light, since they allow a precise phase modulation of the incident beam without changing its amplitude [9]. The molecules of the liquid crystal tilt in response to an applied voltage, so the extraordinary refractive index of the material and therefore the phase of the beam can be controlled at each pixel. Independent voltages are sent to the display in the form of a two-dimensional gray-level mask [9], which contains Fourier transform information of the desired pattern of traps [10].

The dynamic modulation of the light provided by the SLM can however introduce undesired temporal fluctuations in both the phase and the intensity of the beam, and can ultimately degrade the trap performance [11,12]. Although holographic traps have been used for force measurements [13–15], their use could arguably compromise the reliability of quantitative experiments when accuracy and stability are key [16].

The phase of the reflected beam in a phase-only SLM is controlled solely by the orientation of the LC molecules, whose response is, in turn, dependent on the applied voltage and on the viscosity and elasticity of the liquid crystal mixture [17]. If the voltage is modulated quickly enough, the LC molecules sense only its average value, whereas modulations slower than the relaxation time of the LC (determined by its viscosity and elasticity) are followed by the molecules, resulting in a time-dependent phase flicker [17–20].

Unfortunately, SLMs typically require the application of a time-varying voltage to operate. One timescale involves the refresh frequency of the kinoform displayed on the LC (generally at video rate), which makes the display turn off for a short period of time and back on [21,22]. More importantly, because charge accumulation on the LC walls occurs with DC voltages, degrading device performance [23], the applied voltage must change sign (typically at hundreds of Hertz within each refresh period). This modulation can lead to modulation of the phase, with differences in LC response depending on whether the modulator is digitally or analog-addressed [19].

In analog-addressed SLMs, the molecules are subjected only to the charge-balancing switching of the driving voltage. In this case, the amplitude of the signal, the parameter that controls the tilt angle of the LC molecules, can take on continuous values within an operating voltage range. By contrast, digitally-addressed SLMs are binary in nature, and require a more complex mechanism to modify the signal amplitude, which considerably increases the fluctuations inside the LC cell [19]. Digital backplanes provide exclusively two different voltage levels and any intermediate value must be achieved through pulse-width modulation (PWM). In PWM a combination of square waves of varying duration is used within each refresh period to obtain a mean voltage equivalent to the analog value required by the LC to provide the desired phase change.

Here, we provide evidence that the use of digital technology for driving the SLM can result in lower stability of the phase, and ultimately in a lower trap pointing stability than analog addressing. However, even in this case, the use of appropriate addressing schemes can reduce the spatial instability of holographic tweezers to acceptable levels.

Finally and most importantly, we show that the resulting stability of holographic traps generated by analog-addressed SLMs is comparable to conventional, non-holographic tweezers. This suggests the capability of holographic traps for precision force measurements and their potential application to important new fields of research.

2. Experimental setup

We carried out two sets of experiments to study the time-dependent stability of laser beams modulated by SLMs: we first analyzed the stability of the phase delay introduced by the modulators, and, then, we measured the influence of this on the trap position, through the analysis of the motion of holographically trapped particles.

#151453 - $15.00 USD Received 21 Jul 2011; revised 17 Sep 2011; accepted 17 Sep 2011; published 13 Oct 2011

The experiments were conducted using two different holographic optical tweezers setups, one at Simon Fraser University (Canada) and the other at the University of Barcelona (Spain) [11,24]. Infrared (1064 nm) lasers (J20-BL-106C Spectra Physics and YLM-5 IPG Photonics) and liquid-crystal-on-silicon (LCoS) phase-only SLMs (HEO 1080P Holoeye and X10468-03 Hamamatsu) were used. The Holoeye device is a digitally-addressed SLM whereas the Hamamatsu modulator uses analog addressing circuitry.

We have compared the results from three different SLM settings. The Holoeye SLM offers the possibility of selecting several programmable addressing schemes, which differ in their addressing frequencies and in the number of available gray levels (phase levels). Therefore, in addition to the measurements with the analog Hamamatsu SLM (256 gray levels), we studied two different digital addressing sequences of the HoloEye SLM, denoted by the manufacturer as 5-5 (192 gray levels) and 0-6 (64 gray levels), respectively [18]. Here, the first digit indicates the number of equally weighted bitplanes and the second digit indicates the number of binary elements in the addressing sequence.

2.1 Phase measurements

There exist several alternatives for measuring the phase delay introduced by an SLM onto a laser beam [25]. We have used a straightforward method (see Appendix 1) that is appropriate for pure phase SLMs [26].

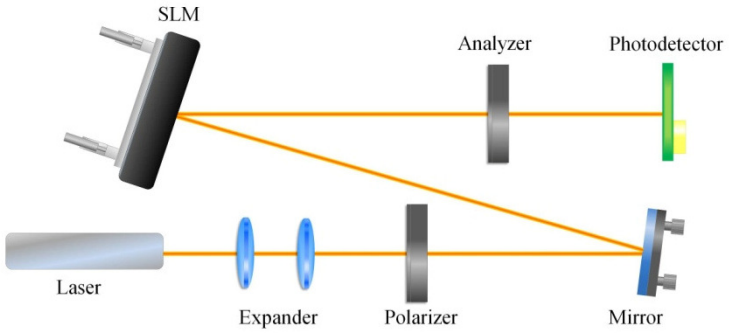

Fig. 1. Setup for phase measurements. Two polarizers at 45° and –45° with respect to the LC alignment direction are inserted before and after the SLM, respectively, and the intensity as read by the photodetector provides information on the phase fluctuations.

The setup is depicted in Fig. 1. Two polarizers at 45° and –45° with respect to the LC alignment direction were inserted before and after the SLM, respectively. The intensity, I, of the reflected light after the analyzer is related to the phase delay ϕ introduced by the modulator to the beam according to [26]:

$$I(\phi) = I_{offset} + I_0 \sin^2\left(\frac{\phi}{2}\right). \quad (1)$$

Here, I_{offset} and I_0 represent the minimum and amplitude of intensity modulations, respectively. A photodetector (QPD, QP154-Q-HVSD, Pacific Silicon Sensors; or PSD PDP90A, Thorlabs) was used to record the temporal fluctuation of this intensity at 15 kHz. The signal was measured for different constant gray levels, that is, for different phase delays imprinted on the SLM. (The mean phase delay introduced by a given gray level is given by the so-called "gamma curve" used for each SLM setting, discussed in Appendix 1). The measured intensities were used to determine the phase as a function of time via Eq. (1). Power spectra of the intensity were calculated, each as an average of 40 independent 1-second measurements.

#151453 - $15.00 USD Received 21 Jul 2011; revised 17 Sep 2011; accepted 17 Sep 2011; published 13 Oct 2011

2.2 Bead position measurements

Positional changes of the holographic traps were indirectly inferred from an analysis of the motion of trapped beads. As the information provided by back-focal-plane interferometry proved to be inconsistent (see Results and Discussion) we utilized high-speed camera tracking. Thus a CMOS camera (PCO, 1200 hs, 1280x1024 pixels, acquisition rate 2500 frames/sec) and a fast back-illuminated Electron Multiplying CCD camera (EM-CCD, Ixon-860, Andor Technologies, 128x128 pixels, acquisition rate ~1.2 kHz) were used to measure the fluctuations in position of a 2 μm diameter polystyrene bead held in a holographic trap.

A single holographic trap was generated offset by tens of microns in both *x* and *y* directions from the zero-order optical center. We used in the two setups the same kinoform, a phase ramp with deliberately different spatial frequencies in the two directions. Differences in position modulations in the *x* and *y* directions were found when using both SLMs. We focus our analysis on modulations in the *x* direction, which were found to be larger, and discuss this further below.

3. Results and Discussion

We first analyzed the temporal stability of the phase of the modulated beam. This quantity is of fundamental importance to trap performance since it controls the trap position.

Examination of the phase versus time plots shows fluctuations for both analog- and digitally-addressed SLMs, with clearly larger modulations for the latter device (Fig. 2, left column). The amplitude of the flicker depends on the imposed gray level (phase delay), with the maximum amplitude of phase modulations occurring at a different phase value for each SLM and setting (Holoeye: gray level = 192, phase delay = 1.7π for 5-5 and gray level = 224, phase delay = 1.75π for 0-6; Hamamatsu: gray level = 64, phase delay = 1.2π), and flickering by as much as 0.31π and 0.16π for the 5-5 and the 0-6 settings, respectively, and $5 \cdot 10^{-4}\pi$ for the Hamamatsu. The larger phase fluctuations observed in our digitally-addressed modulator suggest that holographic traps generated with this SLM will suffer from a lower position stability. However, a large amplitude of phase modulations will not in and of itself cause modulations of trap position (Fig. 3a). Rather, it is the variation in amplitude (Fig. 3b) and/or temporal phase of the modulations among different gray levels that ultimately determines the spatial stability of the optical traps.

For a deeper analysis of temporal stability, we examined the signals with the largest amplitude of phase modulation for each SLM. We computed the power spectrum of the measured $I(\phi)$ signal to obtain information about the frequency dependence of the phase noise introduced by the modulator (Fig. 2, right column). For the analog-addressed device, the SLM introduces peaks at 240 Hz and 480 Hz (Fig. 2(a)), which, according to the manufacturer, correspond to the addressing frequencies of the SLM electronics [27]. For comparison, we included in this plot the spectrum of the laser alone. Its characteristic flat spectrum is affected by the noise introduced by the detector at higher frequencies (~6 kHz), and by the transparency of the silicon photodiode, which acts as a band-pass filter with f_{3dB} = 6.7 kHz (close to that found by others [28]).

#151453 - $15.00 USD Received 21 Jul 2011; revised 17 Sep 2011; accepted 17 Sep 2011; published 13 Oct 2011

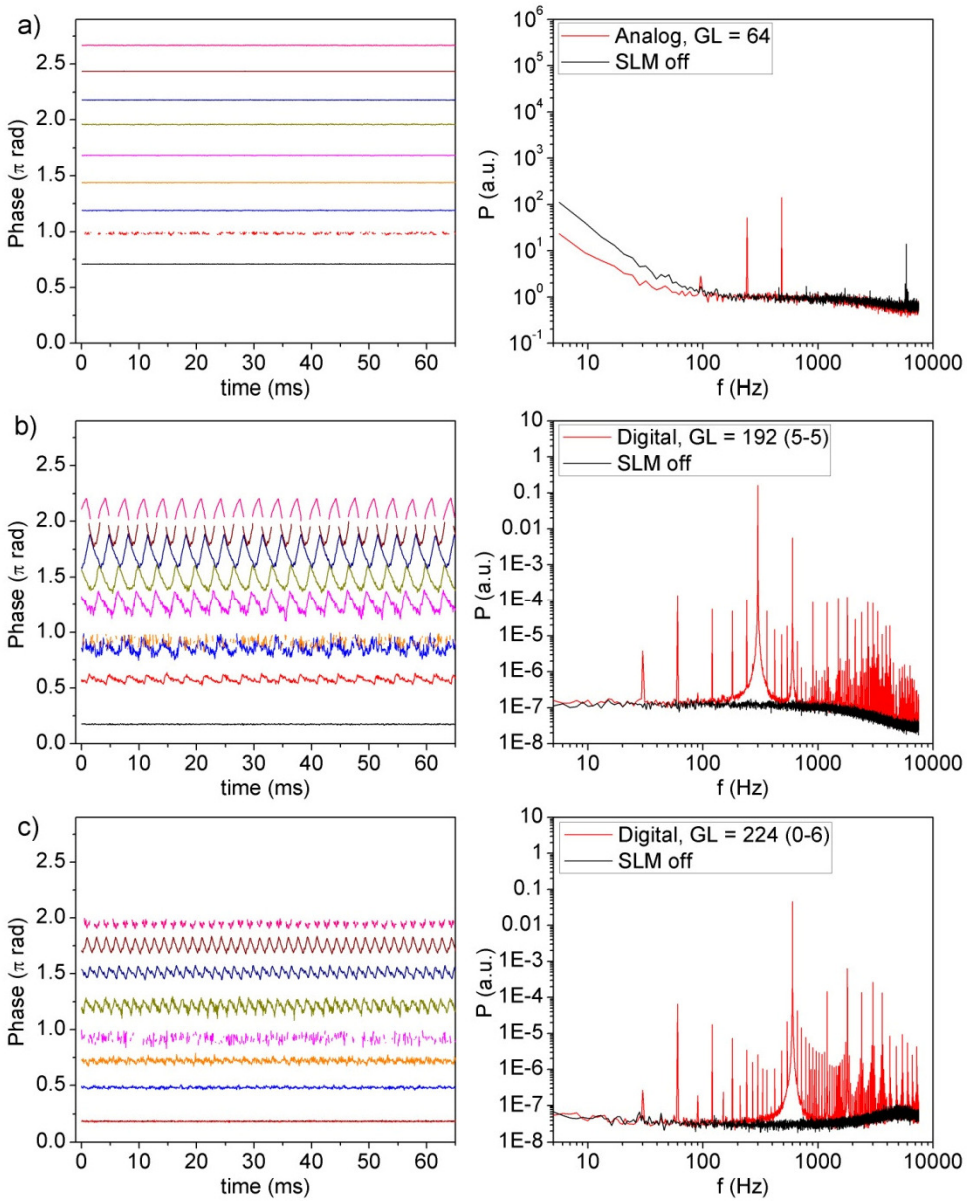

Fig. 2. Left column: phase variation as a function of time for (a) the analog-addressed SLM, (b) the 5-5 setting of the digitally-addressed SLM and (c) the 0-6 setting of the digitally-addressed SLM. In each plot, different curves correspond to different gray levels: 0 (bottom), 32, 64, 96, 128, 160, 192, 224 and 255 (top). Missing data points are due to the fact that Eq. (1) is fit to mean intensity values; therefore, measured intensities greater than (I_{offset} + I_0) or less than I_{offset} (resulting from phase delays of π and 2π, respectively) cannot be converted to phase delays. Right column: for each SLM setting, a power spectrum of the trace with the largest phase modulation shows the frequency dependence of $I(\phi)$ modulation.

Discrete frequency peaks also appear at the addressing frequency when using the digitally-addressed SLM (f_0 = 300 Hz for the 5-5 setting, and f_0 = 600 Hz for the 0-6 setting). In this case, however, the amplitude of the noise is considerably larger and, in addition to the

#151453 - $15.00 USD Received 21 Jul 2011; revised 17 Sep 2011; accepted 17 Sep 2011; published 13 Oct 2011

addressing frequency, oscillations also appear at 60 Hz, due to the display refresh, and overtones of both fundamental modes.

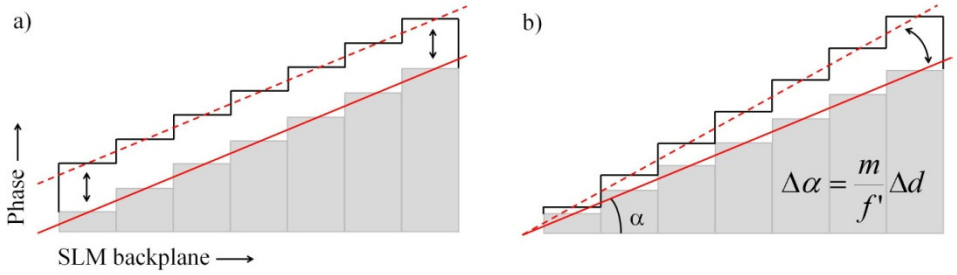

Fig. 3. (a) Phase modulations of equal amplitude that are synchronous will not change the phase gradient, maintaining the spatial frequency of the kinoform. In contrast, phase modulations that are asynchronous and/or (b) differ in amplitude can alter the phase gradient. In this schematic example, temporal variation of the angle α leads to a modulation of the trap position d, where f' is the objective's focal length and m is the magnification of the telescope used to image the SLM onto the objective's entrance pupil.

The large number of peaks at higher frequencies for the digitally-addressed SLM is associated with the pulse-width modulation of the driving voltage amplitude. In PWM, the time spent at each of the two voltages of the supplied digital signal is modulated to generate intermediate time-averaged voltages. Dwell times in each state are fractions of the address cycle time $1/f_0$ and give rise to higher frequency peaks in the power spectrum. The dominant timescale, however, is that of the fundamental mode, where modulation is slowest. At higher frequencies, the viscosity of the LC results in smaller amplitudes of LC molecule reorientation in response to voltage changes, and this gives rise to lower noise. This same effect makes the 0-6 setting, driven at a higher addressing frequency, more stable compared to the 5-5 setting (or to the 22-6 setting with f_0 = 120 Hz, as observed in [11]).

We next assessed how these phase fluctuations translated into trap position instabilities and how the latter depended on the SLM electronics and settings. In principle, trap positions can be measured directly by monitoring the back-reflection of laser foci from the coverslip of the trapping chamber. We previously used this method to characterize the position modulations of holographically created traps, but modulations in intensity and shape of the foci can reduce the accuracy of high-resolution tracking algorithms [12]. Instead, here we studied the motion of trapped particles as probes for the spatial and temporal modulations of these holographically created traps.

As shown in [29], any periodic perturbation dragging a trapped particle appears in the distinctive Lorentzian shape of the power spectrum as a single peak at the oscillation frequency. In particular, the perturbation introduced by the modulator shows up as multiple spikes at the addressing frequency and overtones [11]. The height of these peaks is intimately connected with the amplitude of the trap motion (see Appendix 2), thus providing a means to quantify the pointing stability.

In conventional optical tweezers, these stability measurements would be performed using back-focal-plane interferometry (BFPI) for position detection. The technique is popular due to its high temporal and spatial resolution for position tracking. However, previous results using HOTs [11] had warned us that the amplitude of the bead oscillation obtained from the height of power spectrum peaks may differ significantly from the direct observation of motion with a high-speed camera. The problem is related to the presence of other traps which can interfere, in and out of phase, with the light scattered by the trapped particle at the back focal plane of the collecting lens [12].

In order to prevent undesired interference, here we used a pinhole at a plane conjugate to the sample to eliminate spurious light entering the trapping chamber from zero and higher

#151453 - $15.00 USD Received 21 Jul 2011; revised 17 Sep 2011; accepted 17 Sep 2011; published 13 Oct 2011

diffraction orders. Despite this filtering, there are inconsistencies in our results, in which peaks appear in the BFPI power spectra that are not observed with high-speed camera tracking (both techniques with similar resolution) and the magnitudes of peak heights in the x and y directions are dependent on the presence of the pinhole. Furthermore, the height of the peaks at f_0 increased for increasing laser powers, indicating a larger relative motion of the trapped particle (see below), which is incongruous with the resulting stiffening of the trap.

In BFPI, deflection is normalized by intensity to give displacement, so modulations in intensity may manifest as measured changes in position. Furthermore, any slight temporal delay between acquisition of the deflection and intensity readings may result in convolution of the temporal fluctuations in these independent values, and may be a possible explanation for the failure of BFPI to capture correctly the position modulations of the holographic optical trap, as seen by comparison with high-speed camera imaging.

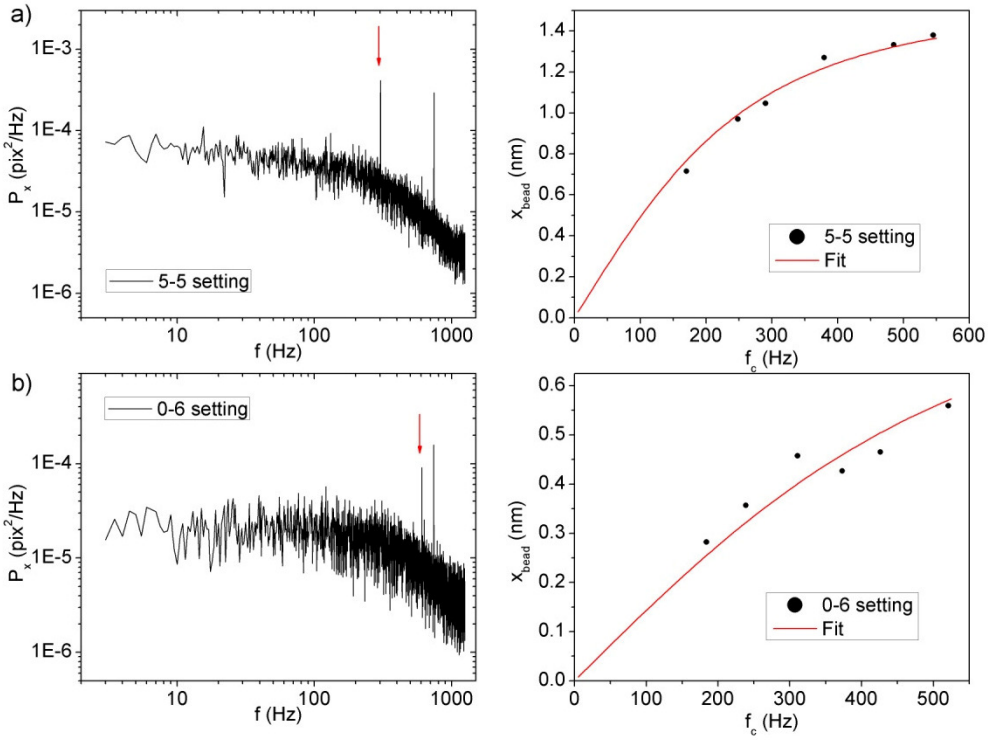

Fig. 4. Left column: power spectra of trapped bead position for different digitally-addressed SLM settings: (a) 5-5 and (b) 0-6. The SLM peak appears at f_0 = 300 Hz and f_0 = 600 Hz, respectively (red arrows). The peak at 742 Hz is caused by a fan in the high-speed camera. Right column: the amplitude of the oscillation obtained from the peak height is plotted for traps with different corner frequencies. The fit of Eq. (3) to the experimental results gives the trap motion, x_0.

Instead of BFPI, we therefore used high-speed cameras to provide a direct observation of trapped particle motion. We first present the results for the digitally-addressed SLM. A typical spectrum of a holographically trapped bead is shown in Fig. 4 for each addressing scheme (5-5 and 0-6). Peaks at 300 Hz and 600 Hz, respectively, appear as clear signatures of beam modulation. The spectra frequently exhibit only one peak, at the fundamental mode of the addressing frequency f_0, indicating that, despite all the noise observed in the phase plots (Fig. 2), the particle's motion is ultimately dominated by a pure sinusoidal modulation: $x_{trap}(t) = x_0 \sin(2\pi f_0 t)$.

The power spectrum of the bead's position in the purely sinusoidal case is [29]:

#151453 - $15.00 USD Received 21 Jul 2011; revised 17 Sep 2011; accepted 17 Sep 2011; published 13 Oct 2011

$$P = \frac{D/\pi^2}{f^2 + f_c^2} + \frac{x_{bead}^2}{2}\delta(f - f_0), \tag{2}$$

where D is the bead's diffusion constant, f_c is the trap roll-off frequency (proportional to trap stiffness), $\delta(f)$ is the Dirac delta function, and the amplitude of the bead oscillation, x_{bead}, is given by (see Appendix 2):

$$x_{bead} = \frac{x_0}{\sqrt{1 + f_0^2/f_c^2}}. \tag{3}$$

This equation shows that the response of the trapped particle is dependent upon the strength of the optical potential. Only when the laser power overcomes the viscous forces imposed by the surrounding fluid does the particle start to follow the trap, and phase fluctuations turn into position fluctuations. Moreover, the existence of a closed mathematical relation between the trap strength and the bead motion provides a means to verify that the cause underlying the appearance of noise in the power spectra is from actual trap movements, and is also a way to determine the trap oscillation amplitude, x_0.

The height of the peak at f_0 in each power spectrum was used to obtain an experimental measurement of x_{bead} (Appendix 2):

$$x_{bead} = \sqrt{2\left(P_{Peak} - P_{therm}\right)\cdot\Delta f}, \tag{4}$$

where P_{peak} and P_{therm} are as defined in Appendix 2. Each data point in Figs. 4(a) and 4(b), right column, is derived from one power spectrum, which is in turn the average of 40 measurements. The experiments were repeated to obtain x_{bead} for traps with different corner frequencies, which were controlled by means of the laser power. The results are fit by Eq. (3) to obtain the value of x_0, as illustrated in Fig. 4. The value for the 5-5 setting, $x_0 = 1.6 \pm 0.3$ nm, is in agreement with previous results [12], while for the 0-6 setting, we determined a smaller oscillation, $x_0 = 0.8 \pm 0.1$ nm, consistent with the improvement seen in the phase measurements. Moreover, the good fit supports the model that the physical mechanism by which peaks show up in the spectra is indeed a physical oscillation of the trap. The error in x_0 corresponds to the standard deviation of x_0 values determined in this manner from measurements on three different beads.

The flicker of the analog-addressed modulator was, by contrast, barely detectable and therefore more difficult to quantify (Fig. 5(a)). Only for large laser powers did peaks appear in the power spectra, and even then, the perturbations were small. In order to assess the system resolution and, therefore, our capability to extract reliable results from these sensitive measurements, we introduced a controlled oscillation as a benchmark.

A piezo stage was used to drive these particle oscillations at a designated frequency, f_{piezo} = 30Hz, and amplitude, x_{piezo} = 20 nm. Simultaneously, the trapped bead was dragged by the fluctuating trap at 480 Hz. Figures 5(a) and 5(b) show two examples of power spectra determined from camera measurements, in which the SLM peak and the piezostage oscillation appear, respectively. In general, however, the two contributions do not appear simultaneously. The SLM effect is present only at high laser powers, when the elasticity of the trap is sufficiently high to drag along the particle, whereas the piezo oscillation becomes visible at low powers when the viscous drag from the fluid motion overcomes the optical force from the laser.

Measurements were carried out for different roll-off frequencies (Fig. 5(c)). The reliability of the results was ensured by measuring the amplitude of the particle motion due to the surrounding fluid in every experiment with two complementary techniques: BFPI and high-speed camera tracking. In this case, BFPI did provide satisfactory results since no fluctuations in the intensity altered the measurement. In addition, since trap calibration can be more

#151453 - $15.00 USD Received 21 Jul 2011; revised 17 Sep 2011; accepted 17 Sep 2011; published 13 Oct 2011

complicated with the high-speed camera [30], we used BFPI to accurately estimate the roll-off frequency.

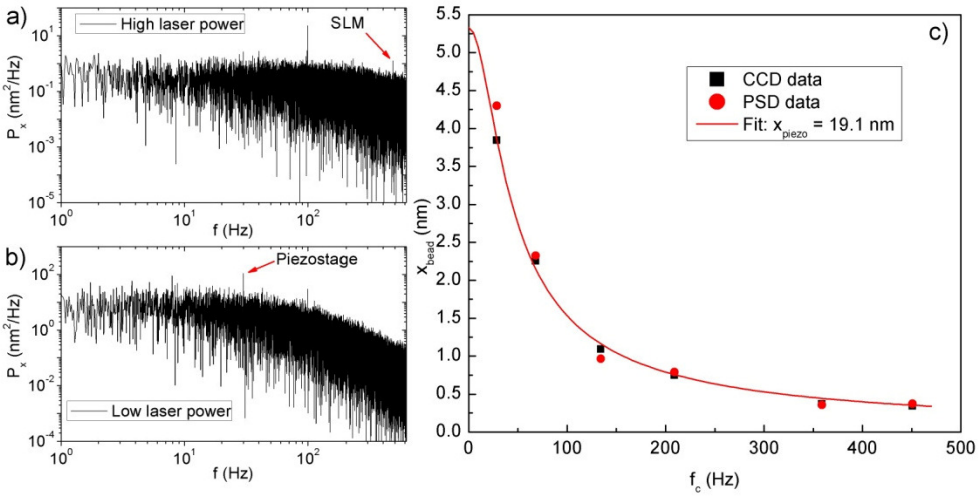

Fig. 5. Power spectra of a 2μm trapped bead determined using a high-speed camera for (a) high and (b) low laser powers, under the simultaneous action of two oscillations: the laser phase fluctuation and a piezostage movement. The peak at 100 Hz is parasitic electronic noise from the room illumination. (c) The amplitude of the piezostage oscillation obtained from the 30 Hz peak from camera data is plotted against the trap roll-off frequency determined from BFPI. The red line is a fit using Eq. (5).

The data and fit shown in Fig. 5(c) correspond to the expected result [29]:

$$x_{bead} = \frac{T \cdot x_{piezo}}{\sqrt{1 + \left(f_c / f_{piezo} \right)^2}}, \tag{5}$$

where $T = 0.27935$ is the value of the piezo stage electronics transfer function at $f_{piezo} = 30$ Hz (the real amplitude of the bead motion was $20 \cdot T = 5.6$ nm). The fitting of the results with Eq. (5) gives us a measure of the amplitude of the piezo oscillation (x_{piezo} ~19.1 nm) that matches the nominal value ($x_{piezo} = 20$ nm).

As a final step, using Eqs. (3) and (4), we determined the amplitude of the SLM-induced trap fluctuation from the peaks at 480 Hz in the same data. Because the amplitude of this motion is so small, control experiments using the piezo stage to induce a range of bead displacements (from ~4 nm to 0.3 nm) were performed in order to evaluate our position resolution.

The result for the analog-addressed SLM ($x_0 = 0.4 \pm 0.1$ nm) seems to be constant for different trap positions in the sample plane. This value is comparable to the position stability observed in the most stable non-holographic tweezers (with external optics also in air) [31,32], which indicates that, here, the trap stability is not compromised by the presence of beam modulations.

Interestingly, we found significant differences in position stability along the x and y axes for both modulators. For the 5-5 setting of the digital-addressed SLM, we estimate $2y_0 = 0.9$ nm, while for the 0-6 setting, no peak is detectable in the power spectrum at $f_0 = 600$ Hz, even at the highest laser powers, suggesting that sub-nanometer stability is attainable in the y direction. Similarly, no peaks appeared in the y direction with the analog-addressed device. Because the kinoform used here was asymmetric, we wondered if the increased stability in y was related to the smaller displacement of the holographic trap from the zero order (*i.e.*, to a

#151453 - $15.00 USD Received 21 Jul 2011; revised 17 Sep 2011; accepted 17 Sep 2011; published 13 Oct 2011

shallower phase gradient in y than in x). To test this hypothesis, we repeated these experiments using a "flipped" kinoform, in which the x and y phase gradients were swapped. Although here the phase gradient along y was steeper, the spatial modulations of the trap remained larger in the x direction.

Here, we have focused on characterizing the position instability along the less stable direction, because ultimately, it is the overall movement of the trap that is relevant for precision measurements. By examining only one axis, one might obtain the impression that the digitally-addressed SLM provides exceptionally stable pointing stability, while this is true only in one direction.

Table 1. Experimental results for holographic trap position instability along the less stable axis, for the different addressing schemes used here.

	Hamamatsu	Holoeye 0-6	Holoeye 5-5	Holoeye 22-6 (from [11])
Modulation frequency f_0 (Hz)	480	600	300	120
Total trap displacement (nm) (= $2x_0$)	0.8 ± 0.2	1.6 ± 0.2	3.2 ± 0.6	>5

The values for the trap position instability for both modulators and the different settings analyzed herein are summarized in Table 1. These correspond to pointing instabilities of 0.4 μrad (Holoeye 5-5), 0.23 μrad (Holoeye 0-6) and 0.06 μrad (Hamamatsu). The performance of the analog SLM is similar to that of the most stable non-holographic optical traps, where pointing stabilities of 0.05 μrad have been achieved [32]. These results, jointly with the temporal behavior of the phase, show that: 1) pointing instabilities come from the modulated LC driving voltage; 2) these fluctuations are larger for our digitally-addressed SLM, which uses pulse-width modulation to adapt the binary applied voltages to small incremental changes in phase; 3) for SLMs with digital electronics, the effect of the flickering decreases with an increase in addressing frequency [17]; and 4) analog-addressed modulators provide similar stability to non-holographic tweezers [31,32].

Additionally, we find that the light intensity in a trap created by both the digitally- and the analog-addressed SLMs is modulated in time, as seen by a peak at f_0 in the power spectrum of intensity modulations from a trapped particle recorded using BFPI (data not shown and [11,12]). The influence of these modulations on force measurements has not been thoroughly investigated, though it has been demonstrated that the use of a time-averaged intensity provides correct force values [14]. Furthermore, because intensity fluctuations do not give rise to peaks in position variance at the modulation frequency [33], the analysis producing the results presented in Table 1 should be unaffected by modulations in trap intensity.

Our digitally-addressed SLM does exhibit less stability than the analog-addressed SLM, but the large phase fluctuations observed surprisingly do not give rise to equivalent instabilities of the trap position. Although still unknown, the reason for this lower than expected position modulation may lie in the somewhat synchronous modulations across gray levels that occur with this digital addressing scheme, giving a predominant effect more like Fig. 3(a) than Fig. 3(b). In any case, we have observed that improvements can be achieved by selecting among available digital addressing schemes (each corresponding to a different addressing rate). It is possible to reduce the amplitude and alter the frequency of the SLM-induced flicker [11,18,20]. Shorter sequences give rise to higher addressing frequencies, which improves the trap performance. We have previously shown an improvement in performance by changing from 22 to 6 (120 Hz addressing) to 5-5 (300 Hz addressing) [11,12], and here, we have found further improvement in the temporal stability by using the 0-6 setting (600 Hz addressing). These findings are consistent with the fact that a shorter temporal sequence permits a higher repetition rate in a frame period and therefore, less relaxation of the liquid crystals between addressing pulses. However, the shorter sequence significantly reduces the number of accessible gray levels from 192 (5-5) to 64 (0-6), which

#151453 - $15.00 USD Received 21 Jul 2011; revised 17 Sep 2011; accepted 17 Sep 2011; published 13 Oct 2011

can have a strong effect on the efficiency of diffraction into the desired first-order beam, particularly at larger steering angles [11]. In addition, due to the design of the modulator's addressing scheme, the 0-6 setting has the disadvantage of not being able to modulate 1064 nm light by a full 2π (see Appendix 1).

The reduction of the phase flickering for increasing addressing frequencies in the digitally-addressed SLM suggests that a further improvement of the trap position stability might be possible with SLMs based on alternative technologies permitting higher addressing rates [17]. All these various considerations should be taken into account when designing experiments requiring precision positioning with HOTs.

4. Conclusions

Analog-addressed SLMs provide a high stability to the modified laser beam when generating holographic optical traps. Measurements of the phase of the modulated beam allowed us to explain the fluctuations observed in the power spectra of holographically trapped beads. The oscillations of the electronic signal sent to the LC are the root cause of these instabilities. With digitally-addressed modulators these fluctuations can dominate the motion of the trapped sample depending on the addressing frequency of the electronics, whereas in the analog-addressed devices, the oscillations are notably reduced, so they do not introduce visible effects on the stability of the trap. Digitally-addressed SLMs offer, in general, reasonable performance, which can be further improved with higher speed addressing [17]. Analog-addressed SLMs, on the other hand, can provide stability comparable to that of non-holographic traps. With the added benefit of real-time positioning of independent traps in three dimensions, a feature not possible in conventional multi-trap optical tweezers instruments, our results demonstrate the advantages to using HOTs for precise quantitative experiments for a wide range of applications.

Appendix 1

For a phase-only SLM, phase modulation can be extracted from intensity readings and does not require an interferometric or diffraction-based measurement. For incoming light linearly polarized at 45° degrees with respect to the extraordinary axis of the SLM nematic liquid crystal molecules, only the extraordinary component of the electric field is modulated by the SLM, while the ordinary component is unaltered. At the exit, light is thus elliptically polarized, with the degree of ellipticity depending on the phase shift ϕ introduced in the modulated component. It follows that the intensity after a second polarizer with its transmission axis at −45° has the expression of Eq. (1). A minimum intensity ($I_{min} = I_{offset}$) is read out when no delay is introduced by the SLM (when the SLM is off or when $\delta = 2m\pi, m \in \mathrm{Z}$), as light will emerge linearly polarized with the same orientation as the incoming light (taking into account a double reflection by the mirror before the SLM and the backplane mirror behind the LC cell) and thus will be blocked by the crossed analyzer. On the contrary, a delay $\delta = (2m+1)\pi, m \in \mathrm{Z}$ will rotate the polarization by 90°, and the intensity after the analyzer will be maximum ($I_{max} = I_{offset} + I_0$).

#151453 - $15.00 USD Received 21 Jul 2011; revised 17 Sep 2011; accepted 17 Sep 2011; published 13 Oct 2011

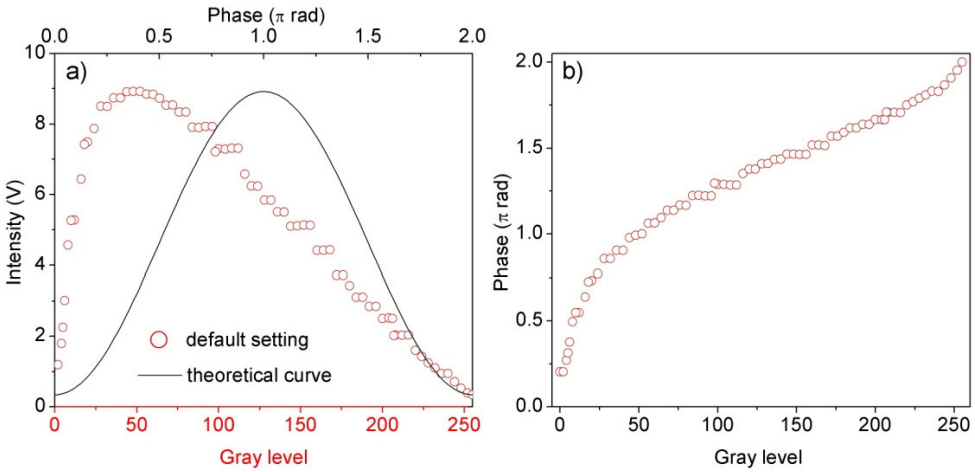

Fig. 6. Determination of the default gamma curve for the Holoeye SLM in the 0-6 addressing scheme. (a) Mean intensity measured for different constant gray levels (red circles) and sine squared theoretical curve from Eq. (1) (black line) after determination of I_0 and I_{offset} from the experimental data. The divergence between these curves shows that gray level and phase delay are not linearly related in this default setting. (b) The default gamma curve, extracted from part (a), gives a nonlinear relation between phase and gray level, not the desired outcome.

We do not have, however, direct control over ϕ but over the gray level, which is used by the SLM to generate such a phase delay through the applied voltage signal according to the addressing scheme. Unfortunately, there is often a non-linear relationship between phase and gray level [9], so the phase – gray-level curve (the so-called gamma curve) needs to be determined and linearized by properly modifying the internal look-up-table (LUT) of the SLM controller. This LUT is provided by some manufacturers to ensure a linear response of the SLM with gray levels. For other SLMs (such as the Holoeye SLM used here), a gamma curve that provides a linear relationship between phase and gray levels is not provided, and, because it can vary with addressing mode and wavelength of operation, it must be determined by the end user. We now outline how to optimize the gamma curve when trying to determine phase modulation from intensity measurements through Eq. (1).

The mean intensity for each gray level (as measured by the photodetector) is represented by a red circle in Fig. 6(a), when using the Holoeye SLM in the 0-6 addressing mode with the default 0-6 gamma curve. We clearly see that the sine squared response predicted by Eq. (1) is deformed by the nonlinear relationship between the gray level and the phase. Nonetheless, the maximum intensity, I_{max}, still corresponds to linear polarization parallel to the analyzer (π phase shift), while I_{min} corresponds to a crossed linear polarization (zero or 2π phase shift). The intermediate intensities correspond to elliptically polarized light given by intermediate phase shifts according to Eq. (1), where $I_{offset} = I_{min}$ and $I_0 = I_{max} - I_{min}$. Thus, if we plot how intensity changes with phase (black line in Fig. 6(a)), we can determine the phase shift ϕ that occurred for each gray level by means of its intensity I, through:

$$\phi = 2 \cdot \sin^{-1} \sqrt{\frac{I - I_{offset}}{I_0}}. \qquad (6)$$

Figure 6(b) shows the dependence of the phase with the gray level deduced from this adjustment. We can clearly see a non-linear behavior and that for this addressing setting the phase shift extends only from ~0.2π το 2π. (For the 5-5 addressing scheme, the default gamma curve provides a much more linear gray scale - phase relation over a 2π range for 1064 nm light.)

#151453 - $15.00 USD Received 21 Jul 2011; revised 17 Sep 2011; accepted 17 Sep 2011; published 13 Oct 2011

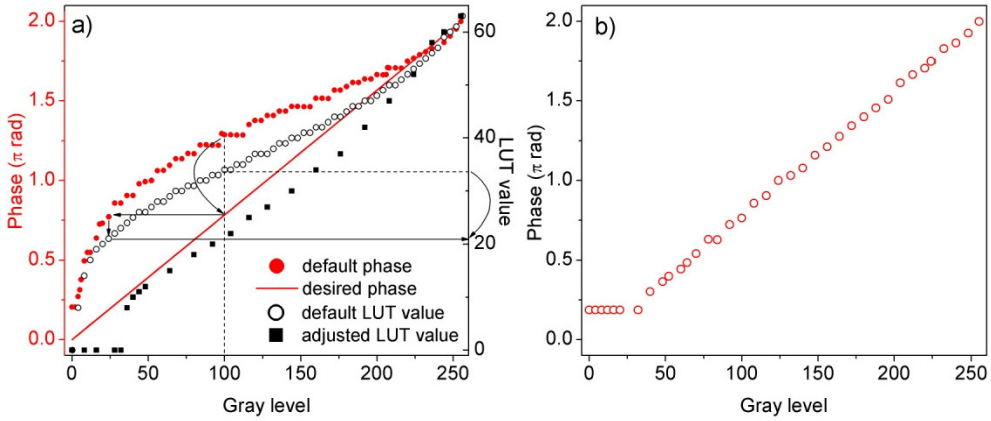

Fig. 7. (a). In order to change the old phase values (filled red circles, left axis) to the desired phase values (red line, left axis), the default LUT value assigned to each gray level (open black circles, right axis) needs to be changed. The filled black squares (right axis) correspond to the new LUT values after adjustment. (b). Resulting phase vs. gray level plot for 0-6, demonstrating the correct linear relation between these two parameters. Note, however, that this setting does not provide a full 2π phase modulation for 1064 nm light.

To obtain a linear relationship between phase and gray level, for each gray level, the correct LUT value must be assigned such that the desired phase delay is generated at the SLM. For instance, as shown in Fig. 7(a) for a gray level of 100, in order to change the corresponding phase delay from 1.28π (default) to 0.78π (desired), we must modify the LUT value for this gray level from 34 to 21. By performing the measurements at small increments of gray scale, we are able to provide new LUT values that lead to a linear gamma curve (Fig. 7(b)). This modified, improved gamma curve was used for all 0-6 measurements reported in this work.

Appendix 2

The amplitude of the particle oscillation in Eq. (3) can be readily derived from the equation of motion governing the dynamics of the system in the absence of thermal noise:

$$m\ddot{x}(t)+\gamma\dot{x}(t)+k\left(x(t)-x_{trap}(t)\right)=0, \tag{7}$$

where $x(t)$ is the particle's position at time t, m is the particle mass, γ is the viscous drag coefficient, k is the harmonic trap stiffness, and the trap motion is described by a pure sine with frequency f_0 : $x_{trap}(t)=x_0\sin(2\pi f_0 t)$. At the timescales of the measurements presented here, the viscosity of the fluid typically overdamps the inertial forces of the particles in it [34], which translates into a small Reynolds number (Re<<1). This guarantees that the first term in Eq. (7) vanishes, so the final expression is simplified to:

$$\gamma\dot{x}(t)+kx(t)=kx_{trap}(t). \tag{8}$$

The general solution is obtained as a combination of two terms: a transient component with a characteristic exponential decay, and a stationary solution given by sinusoidal motion with frequency f_0. The decay time in the former term, $\tau\equiv 2\pi\gamma/k$, takes values on the order of milliseconds, meaning that this contribution becomes relevant at several kHz (negligible for the timescales analyzed in the power spectra presented here). Thus, the final solution to Eq. (8) is given by the stationary term, where the amplitude corresponds to Eq. (3):

#151453 - $15.00 USD Received 21 Jul 2011; revised 17 Sep 2011; accepted 17 Sep 2011; published 13 Oct 2011

$$x(t) = x_{bead}\sin\left(2\pi f_0 t + \phi\right) = \frac{x_0}{\sqrt{1+{f_0^2}/{f_c^2}}}\sin\left(2\pi f_0 t - \arctan\left(\frac{f_0}{f_c}\right)\right). \quad (9)$$

Here, f_c is the roll-off frequency, given by $f_c = k/2\pi\gamma$ (=1/τ). As explained in Section 3, the value of x_{bead} was experimentally obtained from the height of the peaks in the power spectra. Eq. (4) was used for this purpose. We followed a similar approach to that in [29] to obtain this formula.

The temporal Fourier transform of Eq. (9) is given by:

$$\tilde{x}(f) = x_{bead}e^{i\phi}\frac{\delta(f+f_0)-\delta(f-f_0)}{2i}, \quad (10)$$

where $\delta(f)$ is the Dirac delta function. Then, the one-sided power spectrum associated with the oscillation corresponds to a delta function at frequency f_0:

$$P(f) = \frac{2\left|\tilde{x}(f)\right|^2}{T_{msr}} = \frac{x_{bead}^2}{2}\delta(f-f_0). \quad (11)$$

Here, T_{msr} is the measurement time for each power spectrum. The integral under the curve is given by $x_{bead}^2/2$, which can be connected to the experimental measurement obtained from the area under the peak, A, as follows:

$$A = \left(P_{peak} - P_{therm}\right)\Delta f = \frac{x_{bead}^2}{2}. \quad (12)$$

The peak height P_{peak} is integrated above the thermal noise background P_{therm} (determined by a Lorentzian fit to the power spectrum) and the frequency spacing is $\Delta f = 1/T_{msr}$. From this last equation one obtains Eq. (4).

Acknowledgements

Astrid van der Horst initiated investigations of HOT stability at SFU. This work has been partly funded by the Spanish Ministry of Education and Science (FIS2007-65880 and FIS2010-16104; EM-B), by the Natural Sciences and Engineering Research Council of Canada (NSERC; NRF) and by a grant from the Human Frontier Science Program (RGP-2007; NRF). AF acknowledges an FI grant from the Generalitat de Catalunya.

#151453 - $15.00 USD Received 21 Jul 2011; revised 17 Sep 2011; accepted 17 Sep 2011; published 13 Oct 2011